Journal of Science and Technology in Civil Engineering NUCE 2019. 13 (2): 12–23

STATIC ANALYSIS OF FOUR-PARAMETER FUNCTIONALLY GRADED PLATES WITH GENERAL BOUNDARY CONDITIONS

Hoang Thu Phuong[a,*], Tran Huu Quoc[a], Ho Thi Hien[a]

[a]*Faculty of Building and Industrial Construction, National University of Civil Engineering, 55 Giai Phong road, Hai Ba Trung district, Hanoi, Vietnam*

Article history:
Received 07/12/2018, Revised 08/03/2019, Accepted 23/04/2019

Abstract

In this study, the Ritz variational method is used to analyze and solve the bending problem of rectangular functionally graded material plate with general boundary conditions and subject to some types of load distribution over the entire plate domain. Based on the Kirchoff plate theory, the equilibrium equations are obtained by minimizing the total potential energy. The material properties are assumed to be graded through the thickness of the plates according to a power law with four parameters. The accuracy of the solution has been checked and validated through different comparisons to that available literature. A wide variety of examples have been carried out to reveal the influences of different geometrical parameters, FGM power law index, type of load distribution and boundary conditions on the bending responses of the plates. The results show that the gradients in material properties play an important role in determining the response of the FGM plates.

Keywords: FGM; Kirchhoff plate; Ritz method; boundary conditions.

https://doi.org/10.31814/stce.nuce2019-13(2)-02

1. Introduction

Functionally graded materials (FGMs) are a new generation of composite materials, in which the material properties vary continuously and smoothly from one surface to another. This can be achieved by gradually varying the volume power law of constituent materials. The typical FGMs are made of ceramic and metal, the ceramic constituent provides the high-temperature resistance due to its low thermal conductivity, while the ductile metal constituent prevents fracture due to its toughness. Due to their superior physical and mechanical properties, functionally graded materials (FGMs) are widely used in many structural applications such as mechanics, civil engineering, chemical, energy sources, nuclear, automotive fields and shipbuilding industries.

In actual structural applications, functionally graded material may be incorporated in the form of beams, plates or shells as the structural component. It is thus of importance to explore machenical responses of the structures made of FGM. Cheng and Batra [1] investigated the deflections of a simply supported functionally graded polygonal plate by using the first-order shear deformation theory and third-order shear deformation theory. Bending responses of axisymmetric functionally graded circular and annular plates were reported by Reddy et al. [2] based on the first order shear deformation plate

*Corresponding author. *E-mail address:* hoangthuphuong912@gmail.com (Phuong, H. T.)

theory. Talha and Singh [3] studied free vibration and static behavior of functionally graded plates using higher-order shear deformation theory. A continuous isoparametric Lagrangian finite element with 13 degrees of freedom per node is employed for the modeling of functionally graded plates. Thai and Choi [4] presented finite element formulation of various four-unknown shear deformation theories for the bending and vibration analyses of functionally graded plates. Using perturbation techniques, Obata and Noda presented a solution for the transient thermal stresses in a plate made of FGM [5]. The bending analysis of a simply supported exponentially graded rectangular plates subjected to a sinusoidal pressure has been presented by Zenkour [6] using 2D trigonometric and 3D elasticity solutions. Matsugana presented a 2D higher-order deformation theory for investigation of the vibration and stability problems of an FG plate [7] and this theory also used for the evaluation of displacements and stresses in FG plates subjected to thermal and mechanical loadings [8]. Zhao et al. [9] have studied the thermal and mechanical buckling analysis of FG plates according to the first-order shear deformation theory by using the element-free Ritz method. Pradyumna and Bandyopadhyay [10] obtained the linear natural frequencies of FGM curved panels and plates using the finite element method neglecting the heat conduction between ceramic and metal. They discussed the effect of volume fractions of the constituent materials as well as geometry on the natural frequencies. Li et al. [11] studied free vibration of functionally graded material rectangular plates with simply supported and clamped edges in the thermal environment based on the three-dimensional linear theory of elasticity. Kim [12] investigated vibration characteristics of initially stressed FGM rectangular plates in the thermal environment by using Rayleigh-Ritz method based on the third-order shear deformation plate theory to account for rotary inertia and transverse shear strains. Wang et al. [13] presented a unified vibration analysis approach for the four-parameter functionally graded moderately thick doubly-curved shells and panels of revolution with general boundary conditions. An efficient and simple refined shear deformation theory is presented by Meziane et al. [14] for the vibration and buckling of exponentially graded material sandwich plate resting on elastic foundations under various boundary conditions. Zenkour [15] investigated the static response of a simply supported functionally graded rectangular plate subjected to a transverse uniform load by a sinusoidal shear deformation theory and indicated that the gradients in material properties play an important role in determining the response of the FGM plates. Using Navier's solutions and finite element models based on the third order shear deformation plate theory, Reddy [16] studied through-thickness functionally graded plates. The formulation accounts for the thermomechanical coupling, time dependency, and the von Karman-type geometric non-linearity. Daouadji et al. [17] presented a Navier solution of rectangular plates based on a new higher order shear deformation model for the static response of functionally graded plates (FGPs). In which, shear correction factors are not required because a correct representation of transverse shearing strain is given. Quoc et al. [18] studied the bending analysis of functionally graded cylindrical shell panel under mechanical load and thermal effect by finite element method based on the first order shear deformation plate theory. Long et al. [19] presented a new eight-unknow plate theory and investigated the bending and vibration responses of FGM plate by finite element method.

As seen from the above literature survey and to the best of author's knowledge, there are limited investigations on bending analysis of FGM plates with four parameters. In this present study, the mathematical model of four parameters FGM rectangular plates is developed based on Kirchhoff plate theory. By applying the Ritz method, the governing equation can be solved to obtain the static responses of FGM plate with general boundary conditions and subjects to the different types of load distribution over the entire plate domain. The effects of the power-law exponent, length-to-thickness ratio, type of load distribution, and boundary condition on the bending responses of the plates are

examined in details.

2. Theoretical formulation

2.1. Functionally graded material plates

In general, the functionally graded materials are made of two or more constituent phases and their mechanical behaviors are smooth and continuous in one or more directions. It is assumed that Young's modulus $E(z)$, density $\rho(z)$ and Poisson's ratio $\mu(z)$ vary continuously through the thickness direction and can be written in the form of a linear combination:

$$\begin{aligned} E(z) &= (E_c - E_m) V_c + E_m \\ \rho(z) &= (\rho_c - \rho_m) V_c + \rho_m \\ \mu(z) &= (\mu_c - \mu_m) V_c + \mu_m \end{aligned} \tag{1}$$

where the subscripts "c" and "m" represent the ceramic and metallic constituents, respectively, and the volume fraction V_c follows the two general four-parameter power-law distributions [13]:

$$\begin{aligned} \text{FGM}_\text{I} : V_c &= \left[1 - a_1 \left(\frac{1}{2} + \frac{z}{h}\right) + b_1 \left(\frac{1}{2} + \frac{z}{h}\right)^{c_1}\right]^p \\ \text{FGM}_\text{II} : V_c &= \left[1 - a_1 \left(\frac{1}{2} - \frac{z}{h}\right) + b_1 \left(\frac{1}{2} - \frac{z}{h}\right)^{c_1}\right]^p \end{aligned} \tag{2}$$

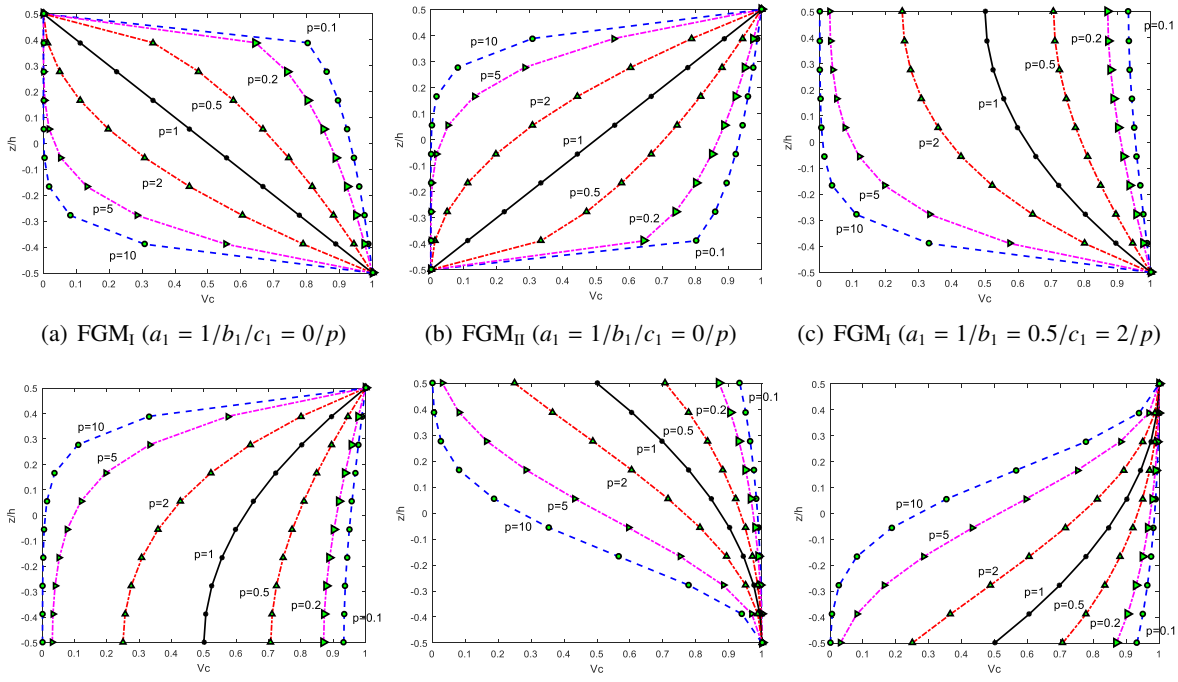

(a) FGM_I ($a_1 = 1/b_1/c_1 = 0/p$) (b) FGM_II ($a_1 = 1/b_1/c_1 = 0/p$) (c) FGM_I ($a_1 = 1/b_1 = 0.5/c_1 = 2/p$)

(d) FGM_II ($a_1 = 1/b_1 = 0.5/c_1 = 2/p$) (e) FGM_I ($a_1 = 0/b_1 = -0.5/c_1 = 2/p$) (f) FGM_II ($a_1 = 0/b_1 = -0.5/c_1 = 2/p$)

Figure 1. Variations of the volume fraction V_c through the thickness of the plate

where p is the power-law exponent and takes only positive values. The sum of the volume fractions of the constituent materials should be equal to one, i.e.,

$$V_c + V_m = 1 \tag{3}$$

When the value of p approaches zero or infinity, one special case of the functionally graded material, namely, the homogeneous isotropic material is obtained. The variations of the volume fraction for different values of the power-law exponent are depicted in Fig. 1.

2.2. Governing equation

According to Kirchhoff plate theory, the displacement field can be given as:

$$\begin{aligned} u(x,y,z) &= u_0 - z\frac{\partial w_0}{\partial x} \\ v(x,y,z) &= v_0 - z\frac{\partial w_0}{\partial y} \\ w(x,y,z) &= w_0 \end{aligned} \tag{4}$$

where u_0, v_0, w_0 are displacement components of a point located on the mid-plane of the plate ($z = 0$) along the (x, y, z) directions, respectively.

The strain-displacement relations of the FGM plate are given as:

$$\begin{aligned} \varepsilon_{xx} &= \frac{\partial u_0}{\partial x} - z\frac{\partial^2 w_0}{\partial x^2} \\ \varepsilon_{yy} &= \frac{\partial v_0}{\partial y} - z\frac{\partial^2 w_0}{\partial y^2} \\ \gamma_{xy} &= \frac{\partial u_0}{\partial y} + \frac{\partial v_0}{\partial x} - 2z\frac{\partial^2 w_0}{\partial x \partial y} \end{aligned} \tag{5}$$

The constitutive relations can be written as:

$$\begin{Bmatrix} \sigma_{xx} \\ \sigma_{yy} \\ \tau_{xy} \end{Bmatrix} = \begin{bmatrix} Q_{11} & Q_{12} & 0 \\ Q_{12} & Q_{22} & 0 \\ 0 & 0 & Q_{66} \end{bmatrix} \begin{Bmatrix} \varepsilon_{\mathrm{xx}} \\ \varepsilon_{yy} \\ \gamma_{xy} \end{Bmatrix} \tag{6}$$

where

$$\begin{aligned} Q_{11} &= \frac{E(z)}{1-\mu^2(z)}; \quad Q_{12} = \frac{E(z)\,\mu(z)}{1-\mu^2(z)}; \\ Q_{66} &= \frac{E(z)}{2(1-\mu(z))}; \quad Q_{21} = Q_{12}; \quad Q_{22} = Q_{11} \end{aligned}$$

The total potential energy functional Π for a Kirchhoff plate is given by:

$$\Pi = U + V \tag{7}$$

where U is the strain energy functional for bending of the Kirchhoff plate and V is the potential energy functional due to the applied transverse load $q(x, y)$ which can be given as follow

$$U = \int_{\Omega} \int_{-\frac{h}{2}}^{\frac{h}{2}} \left(\sigma_{xx}\varepsilon_{xx} + \sigma_{yy}\varepsilon_{yy} + \tau_{xy}\gamma_{xy}\right) dz dx dy \tag{8}$$

$$V = -\int_{\Omega} q\,(x, y) w\,(x, y)\, dx dy \tag{9}$$

Substituting Eq. (4) and Eq. (5) into Eq. (8) and then substituting Eq. (8) and Eq. (9) into Eq. (7), the total potential energy can be rewritten as:

$$\begin{aligned}\Pi = {} & \frac{A}{2}\int_{\Omega}\left[\left(\frac{\partial u_0}{\partial x}\right)^2 + \left(\frac{\partial v_0}{dy}\right)^2 + 2\nu\frac{\partial u_0}{\partial x}\frac{\partial v_0}{dy} + \frac{1}{2}(1-\nu)\left(\frac{\partial u_0}{\partial y} + \frac{\partial v_0}{dx}\right)^2\right] dxdy \\ & - B\int_{\Omega}\left[\frac{\partial^2 w_0}{\partial x^2}\frac{\partial u_0}{\partial x} + \nu\frac{\partial^2 w_0}{\partial x^2}\frac{\partial v_0}{dy} + \nu\frac{\partial^2 w_0}{\partial y^2}\frac{\partial u_0}{\partial x} + \frac{\partial v_0}{dy}\frac{\partial^2 w_0}{\partial y^2} + (1-\nu)\frac{\partial^2 w_0}{\partial x \partial y}\left(\frac{\partial u_0}{\partial y} + \frac{\partial v_0}{dx}\right)\right] dxdy \\ & + \frac{C}{2}\int_{\Omega}\left[\left(\frac{\partial^2 w_0}{\partial x^2}\right)^2 + 2\nu\left(\frac{\partial^2 w_0}{\partial x^2}\frac{\partial^2 w_0}{\partial y^2}\right) + \left(\frac{\partial^2 w_0}{\partial y^2}\right)^2 + 2(1-\nu)\left(\frac{\partial^2 w_0}{\partial x \partial y}\right)^2\right] dxdy \\ & - \int_{\Omega} q\,(x, y) w_0\,(x, y)\, dxdy\end{aligned} \tag{10}$$

where

$$A = \int_{-\frac{h}{2}}^{\frac{h}{2}} \frac{E\,(z)}{1-\mu^2\,(z)} dz, \quad B = \int_{-\frac{h}{2}}^{\frac{h}{2}} \frac{E\,(z)}{1-\mu^2\,(z)} z dz, \quad C = \int_{-\frac{h}{2}}^{\frac{h}{2}} \frac{E\,(z)}{1-\mu^2\,(z)} z^2 dz$$

3. Analytical solutions

Consider a FGM rectangular plate with length a, width b and thickness h subjects to load contribution $q(x, y)$. The types of boundary condition are taken as Fig. 2.

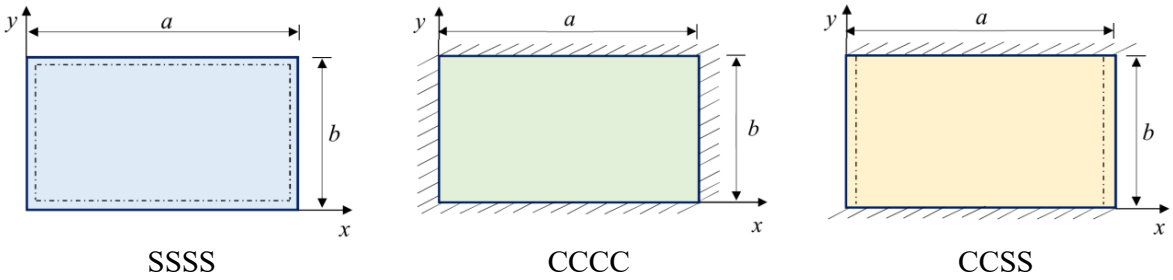

Figure 2. Types of boundary condition

The boundary conditions for an arbitrary edge with simply supported and clamped edge conditions are:

- Clamped (CCCC): $u_0 = v_0 = w_0 = \dfrac{\partial w_0}{\partial x} = \dfrac{\partial w}{\partial y} = 0$ at $x = 0, a$ and $y = 0, b$

- Simply supported (SSSS): $v_0 = w_0 = \dfrac{\partial w_0}{\partial y} = 0$ at $x = 0, a$;

$$u_0 = w_0 = \frac{\partial w_0}{\partial x} = 0 \text{ at } y = 0, b$$

The above boundary conditions are satisfied by the following expansions of the displacements:

$$\begin{aligned} u_0(x,y) &= \sum_{m=1}^{\infty}\sum_{n=1}^{\infty} U_{mn}\frac{\partial X_m(x)}{\partial x}Y_n(y) \\ v_0(x,y) &= \sum_{m=1}^{\infty}\sum_{n=1}^{\infty} V_{mn}X_m(x)\frac{\partial Y_n(y)}{\partial y} \\ w_0(x,y) &= \sum_{m=1}^{\infty}\sum_{n=1}^{\infty} W_{mn}X_m(x)\,Y_n(y) \end{aligned} \tag{11}$$

where U_{mn}, V_{mn}, W_{mn} are arbitrary parameters. The functions $X_m(x)$ and $Y_n(y)$ for the different types of boundary conditions are listed in Table 1 noting that $\lambda_m = m\pi/a$ and $\beta_n = n\pi/b$.

Table 1. The admissible functions $X_m(x)$ and $Y_n(y)$ [14]

	Boundary conditions		The functions X_m and Y_n	
	at $x = 0, a$	at $y = 0, b$	$X_m(x)$	$Y_n(y)$
SSSS	$X_m(0) = X_m''(0) = 0$ $X_m(a) = X_m''(a) = 0$	$Y_n(0) = Y_n''(0) = 0$ $Y_n(b) = Y_n''(b) = 0$	$\sin(\lambda_m x)$	$\sin(\beta_n y)$
CCCC	$X_m(0) = X_m'(0) = 0$ $X_m(a) = X_m'(a) = 0$	$Y_n(0) = Y_n''(0) = 0$ $Y_n(b) = Y_n'(b) = 0$	$\sin^2(\lambda_m x)$	$\sin^2(\beta_n y)$
CCSS	$X_m(0) = X_m'(0) = 0$ $X_m(a) = X_m''(a) = 0$	$Y_n(0) = Y_n'(0) = 0$ $Y_n(b) = Y_n''(b) = 0$	$\sin^2(\lambda_m x)$	$\sin(\beta_m x)$

According to the Ritz method, the equilibrium equations are obtained by minimizing the total potential energy functional Π with respect to the unknown displacement field. Hence, for an extremum of Π with respect to U_{mn}, V_{mn}, W_{mn}, the following conditions are imposed:

$$\frac{\partial \Pi}{\partial U_{mn}} = \frac{\partial \Pi}{\partial V_{mn}} = \frac{\partial \Pi}{\partial W_{mn}} = 0 \tag{12}$$

This yields a system of algebraic equations:

$$\begin{bmatrix} K_{11} & K_{12} & K_{13} \\ K_{21} & K_{22} & K_{23} \\ K_{31} & K_{32} & K_{33} \end{bmatrix} \begin{Bmatrix} U_{mn} \\ V_{mn} \\ W_{mn} \end{Bmatrix} = \begin{Bmatrix} 0 \\ 0 \\ F_{mn} \end{Bmatrix} \tag{13}$$

where

$$
\begin{aligned}
K_{11} &= A\sum_{m=1}^{\infty}\sum_{n=1}^{\infty}\int_0^b\int_0^a\left(2Y_n^2\left(\frac{d^2X_m}{dx^2}\right)^2+(1-\nu)\left(\frac{dX_m}{dx}\frac{dY_n}{dy}\right)^2\right)dxdy\\
K_{12} &= A\sum_{m=1}^{\infty}\sum_{n=1}^{\infty}\int_0^b\int_0^a\left(2\nu X_mY_n\frac{d^2X_m}{dx^2}\frac{d^2Y_n}{dy^2}+(1-\nu)\left(\frac{dX_m}{dx}\frac{dY_n}{dy}\right)^2\right)dxdy\\
K_{13} &= -B\sum_{m=1}^{\infty}\sum_{n=1}^{\infty}\int_0^b\int_0^a\left(Y_n^2\left(\frac{d^2X_m}{dx^2}\right)^2+\nu X_mY_n\frac{d^2Y_n}{dy^2}\frac{d^2X_m}{dx^2}+(1-\nu)\left(\frac{dX_m}{dx}\frac{dY_n}{dy}\right)^2\right)dxdy\\
K_{21} &= A\sum_{m=1}^{\infty}\sum_{n=1}^{\infty}\int_0^b\int_0^a\left(2\nu X_mY_n\frac{d^2X_m}{dx^2}\frac{d^2Y_n}{dy^2}+(1-\nu)\left(\frac{dX_m}{dx}\frac{dY_n}{dy}\right)^2\right)dxdy\\
K_{22} &= A\sum_{m=1}^{\infty}\sum_{n=1}^{\infty}\int_0^b\int_0^a\left(2X_m^2\left(\frac{d^2Y_n}{dy^2}\right)^2+(1-\nu)\left(\frac{dX_m}{dx}\frac{dY_n}{dy}\right)^2\right)dxdy\\
K_{23} &= -B\sum_{m=1}^{\infty}\sum_{n=1}^{\infty}\int_0^b\int_0^a\left(X_m^2\left(\frac{d^2Y_n}{dy^2}\right)^2+\nu X_mY_n\frac{d^2Y_n}{dy^2}\frac{d^2X_m}{dx^2}+(1-\nu)\left(\frac{dX_m}{dx}\frac{dY_n}{dy}\right)^2\right)dxdy\\
K_{31} &= -B\sum_{m=1}^{\infty}\sum_{n=1}^{\infty}\int_0^b\int_0^a\left(Y_n^2\left(\frac{d^2X_m}{dx^2}\right)^2+\nu X_mY_n\frac{d^2X_m}{dx^2}\frac{d^2Y_n}{dy^2}+(1-\nu)\left(\frac{dX_m}{dx}\frac{dY_n}{dy}\right)^2\right)dxdy\\
K_{32} &= -B\sum_{m=1}^{\infty}\sum_{n=1}^{\infty}\int_0^b\int_0^a\left(X_m^2\left(\frac{d^2Y_n}{dy^2}\right)^2+\nu X_mY_n\frac{d^2X_m}{dx^2}\frac{d^2Y_n}{dy^2}+(1-\nu)\left(\frac{dX_m}{dx}\frac{dY_n}{dy}\right)^2\right)dxdy\\
K_{33} &= 2C\sum_{m=1}^{\infty}\sum_{n=1}^{\infty}\int_0^b\int_0^a\left(\begin{array}{l}Y_n^2\left(\frac{d^2X_m}{dx^2}\right)^2+2\nu X_mY_n\frac{d^2X_m}{dx^2}\frac{d^2Y_n}{dy^2}+X_m^2\left(\frac{d^2Y_n}{dy^2}\right)^2+\\+2(1-\nu)\left(\frac{dX_m}{dx}\frac{dY_n}{dy}\right)^2\end{array}\right)dxdy\\
F_{mn} &= \sum_{m=1}^{\infty}\sum_{n=1}^{\infty}\int_0^b\int_0^a qX_mY_ndxdy
\end{aligned}
\tag{14}
$$

4. Results and discussion

4.1. Comparison studies

In this section, the accuracy of the present model is verified by being compared with the literature results. For numerical results, a P-FGM plate made by Al/Al_2O_3 under simply supported boundary condition is considered. The material properties adopted here are:

Aluminum Young's modulus: E_m = 70 GPa, and Poisson's ratio: μ_m = 0.3

Alumina Young's modulus: E_c = 380 GPa, and Poisson's ratio: μ_c = 0.3

The following normalized parameters are used for presenting the numerical results.

$$\bar{w} = 10w_0\left(\frac{a}{2},\frac{b}{2}\right)\frac{E_c h^3}{qa^4}; \quad \bar{\sigma}_{xx} = \frac{h}{aq}\sigma_{xx}\left(\frac{a}{2},\frac{b}{2},\frac{h}{2}\right)$$
$$\bar{\sigma}_{yy} = \frac{h}{aq}\sigma_{yy}\left(\frac{a}{2},\frac{b}{2},\frac{h}{3}\right); \quad \bar{\tau}_{xy} = \frac{h}{aq}\tau_{xy}\left(\frac{a}{4},\frac{b}{4},\frac{h}{2}\right) \tag{15}$$

Table 2. Normalized deflection $\bar{w}$ and stress $\bar{\sigma}_{xx}$ of FGM plates under uniform load

Parameters		Theory			
		NHPSDT [17]	SSDPT [15]	Reddy [16]	Present
$b/a = 1, p = 0$	$\bar{w}$	0.4438	0.4438	0.4438	0.4436
	$\bar{\sigma}_{xx}$	28.7342	28.7342	28.7341	28.7257
$b/a = 3, p = 2$	$\bar{w}$	3.4593	3.4353	3.45937	3.4345
	$\bar{\sigma}_{xx}$	128.728	128.713	128.7283	129.416

The obtained central deflection $\bar{w}$ and normal stress of square plates and rectangular FGM plates under uniform loads are compared with Sinusoidal Shear Deformation Plate Theory (SSDPT) given by Zenkour [15], those reported by Reddy [16] based on Parabolic Shear Deformation Plate Theory (PSDPT) and results by New Hyperbolic Shear Deformation Theory (NHPSDT) by Daouadji et al. [17] in Table 2. It can be seen that the good agreement between the results in this present study and those in the literature has proven the accuracy of the developed approach.

4.2. Parametric studies

After verifying the accuracy of the present solution, the effects of power law index, type of load distribution, side-to-thickness ratio on static responses of FGM plates are discussed in this section.

The material properties of Al/Al_2O_3 are shown as in the comparative example. The plates are subjected to three types of load conditions as shown in Fig. 3.

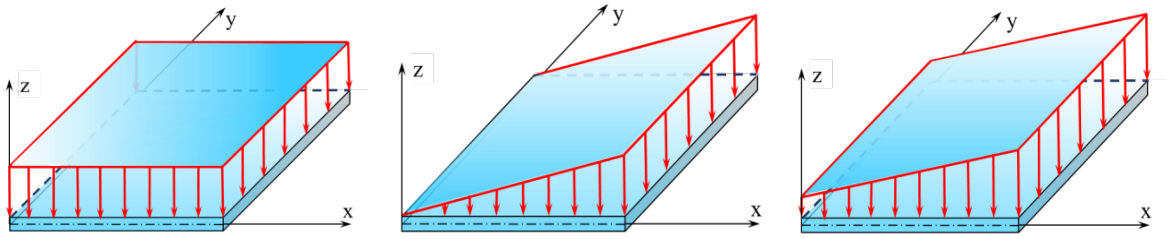

(a) Uniform distributed loading (UD) (b) Hydrostatic distributed loading (HD) (c) Trapezoid distributed loading (TD)

Figure 3. Types of load distributions

Table 3. Deflection $\bar{w}$ and stresses $\left(\bar{\sigma}_{xx}, \bar{\sigma}_{yy}, \bar{\tau}_{xy}\right)$ of FGM plates under UD load

Material	p	$\bar{\sigma}_{xx}$	$\bar{\sigma}_{yy}$	$\bar{\tau}_{xy}$	$\bar{w}$
$\mathrm{FGM}_{\mathrm{I}(a=1/b=0.5/c=2/p)}$	0	−28.725	−28.725	19.461	−0.443
	0.5	−27.355	−26.923	18.659	−0.489
	1	−26.330	−25.590	18.054	−0.533
	2	−25.082	−23.973	17.315	−0.607
	5	−24.445	−23.118	16.947	−0.724
	10	−25.195	−24.138	17.376	−0.788
$\mathrm{FGM}_{\mathrm{II}(a=1/b=0.5/c=2/p)}$	0	−28.725	−28.725	19.461	−0.443
	0.5	−30.989	−31.502	20.846	−0.489
	1	−33.089	−34.101	22.124	−0.533
	2	−36.663	−38.519	24.301	−0.607
	5	−43.001	−45.762	28.331	−0.724
	10	−47.779	−50.057	31.709	−0.788

a. Effect of power law index

Table 3 contains the normalized deflection $\bar{w}$ and stresses $\left(\bar{\sigma}_{xx}, \bar{\sigma}_{yy}, \bar{\tau}_{xy}\right)$ of FGM plates under uniform load $q_0 = 104$ N/m^2 for different values of power-law index p.

It can be seen that increasing the power law index p will reduce the stiffness of the FGM plates, and consequently, leads to an increase in the deflections and stresses. Table 3 also shows that the $\mathrm{FGM_I}$ plates and $\mathrm{FGM_{II}}$ plates have the same deflections but different stresses when they have the same parameters (a, b, c, p), this is because they have the same volume of ceramic and metal but the form distribution of ceramic and metal constituents are different.

The distribution of normalized stresses across the thickness of $\mathrm{FGM_I}$ plates and $\mathrm{FGM_{II}}$ plates are plotted on Figs. 4 to 9.

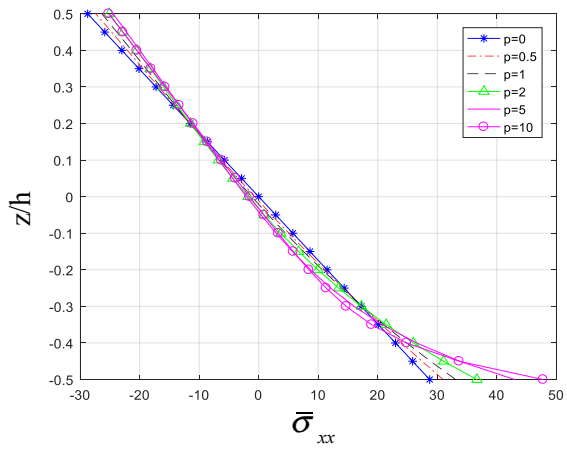

Figure 4. Distribution of $\bar{\sigma}_{xx}\left(\frac{a}{2}, \frac{b}{2}, z\right)$ across the thickness of $\mathrm{FGM}_{\mathrm{I}(a=1/b=0.5/c=2/p)}$ plates

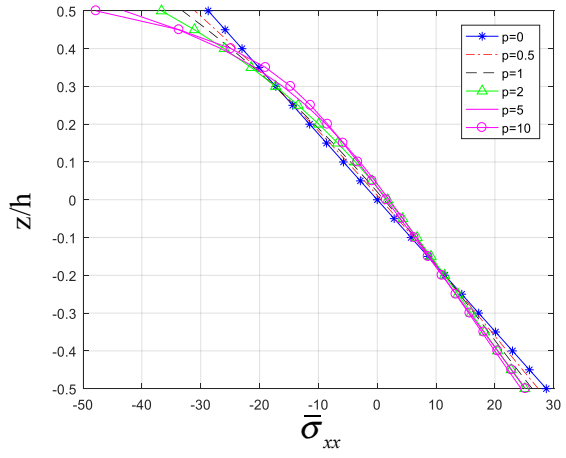

Figure 5. Distribution of $\bar{\sigma}_{xx}\left(\frac{a}{2}, \frac{b}{2}, z\right)$ across the thickness of $\mathrm{FGM}_{\mathrm{II}(a=1/b=0.5/c=2/p)}$ plates

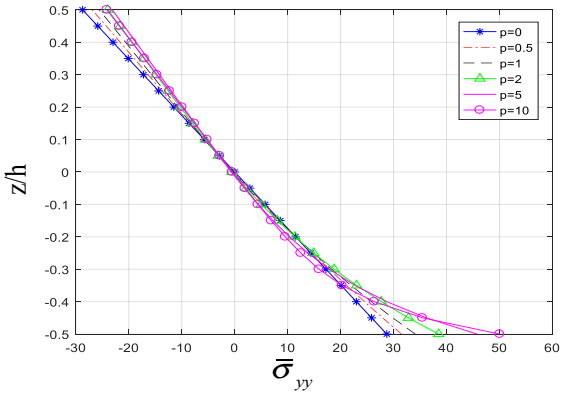

Figure 6. Distribution of $\bar{\sigma}_{yy}\left(\frac{a}{2},\frac{b}{2},z\right)$ across the thickness of $\text{FGM}_{\text{I}(a=1/b=0.5/c=2/p)}$ plates

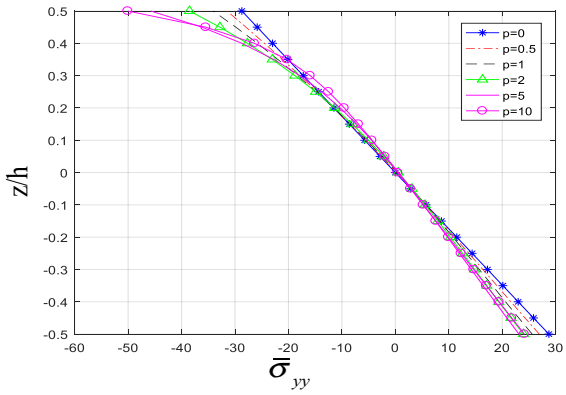

Figure 7. Distribution of $\bar{\sigma}_{yy}\left(\frac{a}{2},\frac{b}{2},z\right)$ across the thickness of $\text{FGM}_{\text{II}(a=1/b=0.5/c=2/p)}$ plates

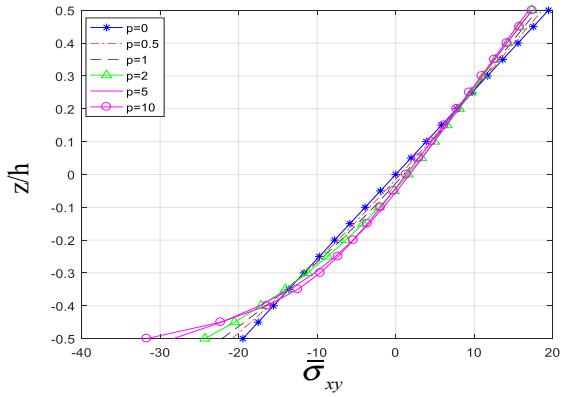

Figure 8. Distribution of $\bar{\tau}_{xy}\left(\frac{a}{2},\frac{b}{2},z\right)$ across the thickness of $\text{FGM}_{\text{I}(a=1/b=0.5/c=2/p)}$ plates

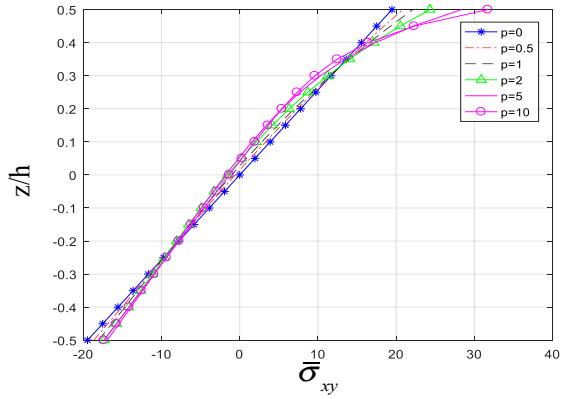

Figure 9. Distribution of $\bar{\tau}_{xy}\left(\frac{a}{2},\frac{b}{2},z\right)$ across the thickness of $\text{FGM}_{\text{II}(a=1/b=0.5/c=2/p)}$ plates

Figs. 4 to 9 show that the distribution of the normal stresses and shear stresses are linear through the thickness of the isotropic plate with zero value at the mid-surface but those distribution in FGM plates are nonlinear with zero value at the other point which depends on the gradient index. As the distributions of volume fraction V_c in FGM_{I} are in the turned direction of the distributions of volume fraction V_c in FGM_{II} leads to the distributions of stresses in FGM_{I} and in FGM_{II} are also in opposite direction.

b. Effect of type of load distribution

Examination of the results displayed in Table 4 reveals the effect of the type of load distribution on the static response of FGM plates.

According to the results, the type of load has so much influence on the central deflection and stress of the plates. It is noticeable that the central deflections and stresses of plates subjected to UD load may be twice those of plates subjected to HD load while those of plates subjected to TD are highest. Table 4 also shows the great influence of the boundary conditions on analyzed deflections and stresses of FGM plates subjected to the mechanical load.

Table 4. Normalized deflection $\bar{w}$ and stresses $\left(\bar{\sigma}_{xx}, \bar{\sigma}_{yy}, \bar{\tau}_{xy}\right)$ of FGM under UD, HD and TD load subjected to various boundary conditions

Boundary conditions	Type of load	$\bar{\sigma}_{xx}$	$\bar{\sigma}_{yy}$	$\bar{\tau}_{xy}$	$\bar{w}$
SSSS	UD	−25.082	−23.9731	7.1264	−0.607
	HD	−12.541	−11.986	3.5632	−0.303
	TD	−150.494	−143.834	42.7581	−3.642
CCCC	UD	−42.013	−40.155	4.3108	−0.211
	HD	−21.006	−20.077	2.1554	−0.105
	TD	−252.080	−240.933	25.8646	−1.267
CCSS	UD	−27.791	−15.167	4.524	−0.288
	HD	−13.895	−7.581	2.262	−0.144
	TD	−166.743	−90.975	27.146	−1.727

c. Effect of side-to-thickness ratio and material anisotropy

The effects of the side-to-thickness ratio (varying a/h from 50 to 100) on the normalized deflections of FGM plates for different values of p are shown in Fig. 10.

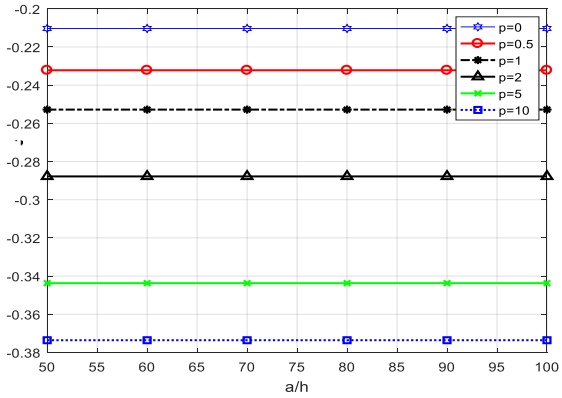

Figure 10. Effect of a/h ratio on the $\bar{w}$ of the FGM plates (SSSS, a/h = 50, UD)

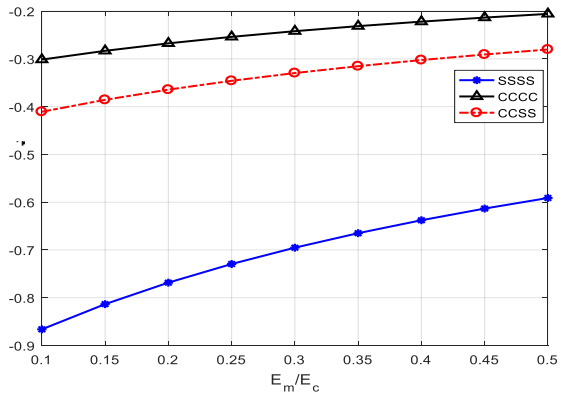

Figure 11. Effect of material anisotropy on the $\bar{w}$ of the FGM plates for different values of p

Fig. 10 shows that the normalized deflection is maximum for the metallic plate and minimum for the ceramic plate while it is unchanged with the increase of side-to-thickness ratio.

Finally, the exact maximum deflections of FGM square plate with SSSS, CCCC and CCSS boundary conditions are compared in Fig. 11 for various ratios of moduli, E_m/E_c (for a given thickness, a/h = 50). This means that the deflections are computed for plates with different ceramic-metal mixtures. It is clear that the deflections decrease smoothly as the volume fraction exponent decreases and as the ratio of metal-to-ceramic moduli increases.

5. Conclusions

In summary, an analytical solution to investigate the static response of functionally graded plates based on Kirchhoff theory and Ritz method is developed. The present numerical results show high

accuracy when compared to those in the open literature. The effect of the power law index, plate side-to-thickness, type of load distribution, and boundary conditions on the static response of FGM plates are investigated. It is revealed that different plates show different stress profiles across the thickness which depend on the variations of material properties in the thickness direction. Thus, the gradients in material properties play an important role in determining the response of the FGM plates.

References

[1] Cheng, Z. Q., Batra, R. C. (2000). Deflection relationships between the homogeneous Kirchhoff plate theory and different functionally graded plate theories. *Archives of Mechanics*, 52(1):143–158.

[2] Reddy, J. N., Wang, C. M., Kitipornchai, S. (1999). Axisymmetric bending of functionally graded circular and annular plates. *European Journal of Mechanics-A/Solids*, 18(2):185–199.

[3] Talha, M., Singh, B. N. (2010). Static response and free vibration analysis of FGM plates using higher order shear deformation theory. *Applied Mathematical Modelling*, 34(12):3991–4011.

[4] Thai, H.-T., Choi, D.-H. (2013). Finite element formulation of various four unknown shear deformation theories for functionally graded plates. *Finite Elements in Analysis and Design*, 75:50–61.

[5] Obata, Y., Noda, N. (1993). Transient thermal stresses in a plate of functionally gradient material. *Ceramic Transactions*, 34:403–410.

[6] Zenkour, A. M. (2007). Benchmark trigonometric and 3-D elasticity solutions for an exponentially graded thick rectangular plate. *Archive of Applied Mechanics*, 77(4):197–214.

[7] Matsunaga, H. (2008). Free vibration and stability of functionally graded plates according to a 2-D higher-order deformation theory. *Composite Structures*, 82(4):499–512.

[8] Matsunaga, H. (2009). Stress analysis of functionally graded plates subjected to thermal and mechanical loadings. *Composite Structures*, 87(4):344–357.

[9] Zhao, X., Lee, Y. Y., Liew, K. M. (2009). Mechanical and thermal buckling analysis of functionally graded plates. *Composite Structures*, 90(2):161–171.

[10] Pradyumna, S., Bandyopadhyay, J. N. (2008). Free vibration analysis of functionally graded curved panels using a higher-order finite element formulation. *Journal of Sound and Vibration*, 318(1-2):176–192.

[11] Li, Q., Iu, V., Kou, K. (2009). Three-dimensional vibration analysis of functionally graded material plates in thermal environment. *Journal of Sound and Vibration*, 324(3-5):733–750.

[12] Kim, Y.-W. (2005). Temperature dependent vibration analysis of functionally graded rectangular plates. *Journal of Sound and Vibration*, 284(3-5):531–549.

[13] Wang, Q., Shi, D., Liang, Q., Pang, F. (2017). Free vibration of four-parameter functionally graded moderately thick doubly-curved panels and shells of revolution with general boundary conditions. *Applied Mathematical Modelling*, 42:705–734.

[14] Meziane, M. A. A., Abdelaziz, H. H., Tounsi, A. (2014). An efficient and simple refined theory for buckling and free vibration of exponentially graded sandwich plates under various boundary conditions. *Journal of Sandwich Structures & Materials*, 16(3):293–318.

[15] Zenkour, A. M. (2006). Generalized shear deformation theory for bending analysis of functionally graded plates. *Applied Mathematical Modelling*, 30(1):67–84.

[16] Reddy, J. N. (2000). Analysis of functionally graded plates. *International Journal for numerical methods in engineering*, 47(1-3):663–684.

[17] Daouadji, T. H., Tounsi, A., Bedia, E. A. (2013). Analytical solution for bending analysis of functionally graded plates. *Scientia Iranica*, 20(3):516–523.

[18] Quoc, T. H., Huan, D. T., Tu, T. M., Tan, N. Q. (2017). Bending analysis of functionally graded cylindrical shell panel under mechanical load and thermal effect-Analytical solution and Finite element model. *Journal of Science and Technology in Civil Engineering*, 11(2):38–46.

[19] Long, N., Quoc, T. H., Tu, T. M. (2016). Bending and free vibration of functionally graded plates using new eight-unknow shear deformation theory by finite element. *Vietnam Journal of Science and Technology*, 54(3):402–415.